Optimal Mode and Droop Setting of Smart Inverters

Temitayo O. Olowu, Adedoyin Inaolaji, Sumit Paudyal, and Arif Sarwat
Florida International University, Miami, USA
Emails: {tolow003, ainao003, spaudal, asarwat}@fiu.edu

***Abstract*—This paper proposes a two-time-scale distribution grid optimal power flow (D-OPF) framework that provides optimal settings of smart inverters' (SIs) modes and droops in coordination with existing legacy voltage control devices. On a slow time scale, the optimal SI modes and droop settings, tap position of voltage regulator/on-load tap changers (VR/OLTC), and capacitor bank status are obtained. On a fast time scale, using the optimal solutions obtained from a slow time scale model, the SIs' optimal active/reactive power dispatch is obtained in a way that ensures the active/reactive power setpoints lie on the SIs' droop. This ensures a feasible implementation at the local controller level. The proposed approach is demonstrated using the IEEE 123-node unbalanced three-phase test feeder and is compared with an existing method of SI mode and droop setting selection in the literature. The results show the feasibility of optimally selecting the SI's modes and settings. Also, compared to the method in the literature, the proposed approach achieves better voltage regulation.**

***Index Terms*—distribution optimal power flow (D-OPF), volt/VAr control (VVC), smart inverter modes, and settings.**

I. Introduction

Smart inverters (SIs) are becoming feasible alternatives for providing voltage and reactive power (Volt/VAr) support in the modern power distribution system. In traditional power systems, legacy grid devices such as on-load tap changers (OLTC) and capacitor banks (CAPs) are used for Volt/VAr control (VVC). However, due to the limitation of mechanical switching, these devices may not be able to mitigate the fast voltage fluctuations caused by photovoltaics (PVs). On the other hand, inverter-based PVs can provide fast, flexible, and precisely controlled active/reactive power support and could be used for voltage control [1]. Therefore, inverter-based PVs can be coordinated with the legacy grid devices to regulate voltage and reactive power in different timescales of operations. Inverter types used for PV applications include string and micro-inverters.

A common approach for implementing VVC is formulating a distribution grid optimal power flow (D-OPF) problem. D-OPF models exist to obtain the setpoints of inverters (e.g., [2, 3]). However, the SI setpoints should be based on local droops as defined in the IEEE-1547 [1], which are not considered in [2, 3]; therefore, the dispatch setpoints obtained from these works may contradict the local droop settings of SIs. A feasible approach to ensure that the SI setpoints are feasible at the local inverter controller level is to account for the SI mode and droop settings in the D-OPF formulation. In this regard, existing works in [4–6] develop SI droop-constrained D-OPF models whose SI setpoints conform to the IEEE 1547. These works, however, are based on predefined SI droop settings, which may be ineffective since the system conditions are always changing. To overcome the sub-optimality issues caused by the fixed droop settings, optimal droop settings of SIs are obtained in [7, 8].

A significant drawback of the aforementioned works in [4–8] is that they assume a predefined SI mode selection, which could lead to sub-optimal solutions since the voltage sensitivities to different SI modes varies due to different X/R values across the feeder [9]. Besides, as per IEEE-1547 [1], SIs can switch between modes (e.g., constant power factor mode, constant reactive power mode, Volt/VAr mode, Volt/Watt mode) based on the prevailing grid parameters. The discrete decision to choose an appropriate SI mode and the piece-wise linear nature of SI droops, as prescribed in the IEEE-1547, pose an inherent mathematical challenge in integrating SI constraints into the D-OPF formulations.

In this context, this paper presents a novel effort to explore multi-mode and multi-droop settings of SIs for coordinated control of SIs and legacy devices at two different timescales. The first stage of the D-OPF that determines the SI modes, SI droop settings, CAPs switching status, and OLTC positions is formulated as a mixed-integer non-linear programming (MINLP) problem. The second stage of the D-OPF, formulated as a non-linear programming (NLP) problem, dispatches the active/reactive power setpoints of the SIs on the droops determined from the first stage. To the best of our knowledge, this is the first attempt to develop comprehensive mathematical models of the SI droops and modes as decision variables in a D-OPF formulation. This allows the D-OPF to optimally select the modes and droop settings of SIs as the system condition varies. Moreover, this ensures that the inverter dispatch solutions lie precisely on the local droops of the SIs as per IEEE-1547 guidelines.

The rest of the paper is structured as follows. The modeling of the SI modes and droop is presented in section II. Section III presents the OPF formulation. The coordination of the SI with the voltage control legacy devices is presented in section IV. Simulation results and analyses are presented in section V, while section VI concludes the paper.

II. Modeling of SI Modes and Droop Settings

This section presents brief mathematical modeling of SI modes and droop settings based on the IEEE-1547-2018 [1].

A. Volt/Watt (VW) Mode

In VW mode, the rate of change in active power injection due to a change in the voltage at the point of interconnection

This work is supported in part by National Science Foundation grant ECCS-2001732 and CNS-1553494. Corresponding Author: T. O Olowu, Florida International University, Miami. Email: tolow003@fiu.edu

(POI) depends on the slope of the VW curve, as shown in Fig. 1a. The SI droop control in the VW mode is expressed as in (1).

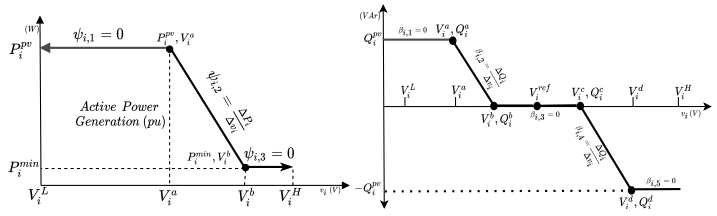

(a) (b)

Fig. 1: (a) Volt/Watt curve (b) Volt/VAr curve

$$P_i^G = \begin{cases} P_i^{pv} & V_i^L \le v_i \le V_i^a \\ P_i^{min} + \psi_{i,2}(v_i - V_i^b) & V_i^a \le v_i \le V_i^b \\ P_i^{min} & V_i^b \le v_i \le V_i^H \end{cases} \quad (1)$$

where for a given node i: $\psi_{i,2} = \frac{P_i^{pv} - P_i^{min}}{V_i^a - V_i^b}$ is the slope of the VW curve, P_i^{pv} and P_i^{min} are the available and the minimum active power generation respectively, $V_i^L \dots V_i^H$ are the SI curve breakpoints, P_i^G is the instantaneous active power dispatch. Using the Heaviside step function as in [7], the piecewise VW droop settings can be modeled as in (2).

$$\begin{aligned} P_i^G = P_i^{pv} \Big[& [\mathbb{H}(v_i - V_i^L) - \mathbb{H}(v_i - V_i^a)] + \\ & \frac{P_i^{min} + (v_i - V_i^b)\psi_{i,2}}{P_i^{pv}} [\mathbb{H}(v_i - V_i^a) - \mathbb{H}(v_i - V_i^b)] + \\ & \frac{P_i^{min}}{P_i^{pv}} [\mathbb{H}(v_i - V_i^b) - \mathbb{H}(v_i - V_i^H)] \Big], \forall\, i \in \mathcal{N}_{pv} \end{aligned} \quad (2)$$

where the Heaviside function $\mathbb{H} : \mathbb{Z} \to \mathbb{R}$ is defined as,

$$\mathbb{H}(a) = \begin{cases} 0, & a < 0 \\ 1, & a \ge 0 \end{cases} \quad (3)$$

In VW mode, the active power constraint can be expressed as $P_i^{min} \le P_i^G \le P_i^{pv}, \quad \forall i \in \mathcal{N}_{pv}$. $\mathcal{N}_{pv}$ is the set of nodes with PV. The instantaneous reactive power Q_i^G is expressed as (4).

$$Q_i^G \le \sqrt[2]{(S_i^{SI})^2 - (P_i^G)^2}, \quad \forall i \in \mathcal{N}_{pv} \quad (4)$$

The reactive power is constrained within $-Q_i^{pv} \le Q_i^G \le Q_i^{pv}, \quad \forall i \in \mathcal{N}_{pv}$, where Q_i^{pv} is the available reactive power and S_i^{SI} is the SI's apparent power rating.

B. Volt/VAr (VV) Mode

The rate of reactive power injection and absorption using the VV mode is determined by the slopes of the VV curve as shown in Fig. 1b. The VV mode can be mathematically expressed as in (5).

$$Q_i^G = \begin{cases} Q_i^{pv} & V_i^L \le v_i \le V_i^a \\ (v_i - V_i^b)\beta_{i,2} & V_i^a \le v_i \le V_i^b \\ 0 & V_i^b \le v_i \le V_i^c \\ (v_i - V_i^c)\beta_{i,4} & V_i^c \le v_i \le V_i^d \\ -Q_i^{pv} & V_i^d \le v_i \le V_i^H \end{cases} \quad (5)$$

where $\beta_{i,2} = \frac{Q_i^{pv}}{V_i^a - V_i^b}$ and $\beta_{i,4} = \frac{Q_i^{pv}}{V_i^c - V_i^d}$ are the slopes of the VV curve within a given voltage range. Using the Heavside step function as in [7], the VV mode can be modeled as expressed in (6).

$$\begin{aligned} Q_i^G = Q_i^{pv} \Big[& [\mathbb{H}(v_i - V_i^L) - \mathbb{H}(v_i - V_i^a)] + \\ & \frac{(v_i - V_i^b)\beta_{i,2}}{Q_i^{pv}} [\mathbb{H}(v_i - V_i^a) - \mathbb{H}(v_i - V_i^b)] + \\ & \frac{(v_i - V_i^c)\beta_{i,4}}{Q_i^{pv}} [\mathbb{H}(v_i - V_i^c) - \mathbb{H}(v_i - V_i^d)] + \\ & [\mathbb{H}(v_i - V_i^d) - \mathbb{H}(v_i - V_i^H)] \Big] \forall i \in \mathcal{N}_{pv} \end{aligned} \quad (6)$$

In VV mode, the reactive power constraint can be expressed as $-Q_i^{pv} \le Q_i^G \le Q_i^{pv}, \quad \forall i \in \mathcal{N}_{pv}$. The available active power is expressed as (7).

$$P_i^G \le \sqrt[2]{(S_i^{SI})^2 - (Q_i^G)^2} \quad \forall i \in \mathcal{N}_{pv} \quad (7)$$

The active power is constrained within $P_i^{min} \le P_i^G \le P_i^{pv}, \quad \forall i \in \mathcal{N}_{pv}$. The VV mode can be operated either in VAr-priority mode (Q-priority) or Watt-priority (P-priority), as shown in Fig. 2a.

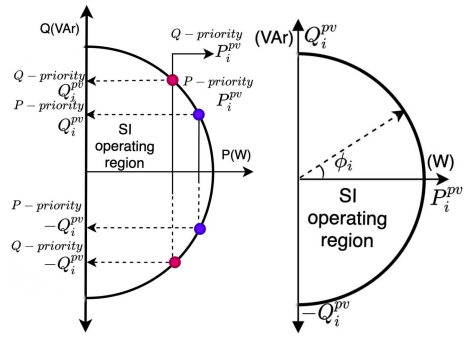

(a) (b)

Fig. 2: (a) SI operating region in Volt/VAr (P/Q priority) mode [10] (b) CPF mode

1) Volt/VAr with reactive power priority (Q-Priority): In the VV Q-priority mode, the reactive power generation/absorption by the SI is prioritized over active power generation. The active power dispatched in this mode is as expressed in (8).

$$P_i^G \le \sqrt[2]{(S_i^{SI})^2 - (Q_i^G)^2}, \quad \forall i \in \mathcal{N}_{pv} \quad (8)$$

where $Q_i^G \le S_i^{SI}$; $P_i^{min} \le P_i^G \le P_i^{pv}$ and $P_i^{curt} = P_i^{pv} - P_i^G$.

2) Volt/VAr with active power priority (P-priority): In VV P-priority mode, the entire active power based on the prevailing irradiance is available for dispatch. The available reactive power dispatch in this mode is as expressed in (9).

$$Q_i^G \le \sqrt[2]{(S_i^{SI})^2 - (P_i^{pv})^2}, \quad \forall i \in \mathcal{N}_{pv} \quad (9)$$

C. Constant power factor (CPF) mode

The CPF mode allows the SI to inject or absorb a fixed amount of reactive/active power in order to regulate the feeder voltage as expressed in (10). Assuming the SI can operate in

two quadrants of active and reactive power dispatch and for a power factor, ϕ_i, between ϕ_i^{min} and ϕ_i^{max} the CPF mode is as shown in Fig. 2b.

$$Q_i^G = P_i^{pv} \tan\phi_i, \quad \forall i \in \mathcal{N}_{pv} \tag{10}$$

III. Optimal Power Flow Formulation

The total voltage deviation, as a result of the voltage control action of the SIs, CAPs, and OLTC/VR, is set as the objective function (OF) as expressed in (11).

$$OF = \min \sum_{i\in\mathcal{N}} \left| \frac{R_i^{eq}\,\Delta P_i^G + X_i^{eq}\,\Delta Q_i^G}{v_i} + \frac{1}{v_i} X_i^{eq} \Delta Q_i^c + \Delta Z(tp_i)\cdot I_0 + Z_0 \cdot \Delta I(tp_i) \right| \tag{11}$$

where $\mathcal{N}$ is the set of all network nodes i. I_0, Y_0, Z_0 are current injection, admittance, and impedance matrix, respectively, prior to tap change. $\Delta I(tp_i), \Delta Y(tp_i), \Delta Z(tp_i)$ are the change in current injection, admittance, and impedance matrix after a tap change at node i. R_i^{eq}, X_i^{eq} are the equivalent resistance and reactance respectively at the point of interconnection, Q_i^c is the reactive power injection of the capacitor bank, v_i is the instantaneous voltage, and the tp_i is the OLTC/VR tap position. The distribution grid is modeled and set as part of the optimization constraints using the power flow equations in (12)-(16) [11].

$$\Delta P_i(v_i,\delta_i) = P_i^G - P_i^L \quad \forall i \in \mathcal{N} \tag{12}$$

$$\Delta Q_i(v_i,\delta_i) = Q_i^G - Q_i^L \quad \forall i \in \mathcal{N} \tag{13}$$

where,

$$\Delta Q_i(v_i,\delta_i) = v_i \sum_{k\in N} v_k(\mathcal{G}_{ik}\cos(\delta_{ik}) + \mathcal{B}_{ik}\sin(\delta_{ik})) \tag{14}$$

$$\Delta P_i(v_i,\delta_i) = v_i \sum_{k\in N} v_k(\mathcal{G}_{ik}\sin(\delta_{ik}) - \mathcal{B}_{ik}\cos(\delta_{ik})) \tag{15}$$

The nodal voltage constraint in the network is as expressed in (16).

$$v^{min} \le v_i \le v^{max}, \quad \forall i \in \mathcal{N} \tag{16}$$

where P_i^L, Q_i^L are the load active and reactive power, $\mathcal{G}_{ik}$,$\mathcal{B}_{ik}$ real and imaginary parts of admittance matrix between nodes i and k, while δ_i is the voltage angle. The control of the discrete-control legacy devices makes this formulation MINLP in nature for the first stage of the D-OPF, which requires solving (11) subject to (17). The second stage, on the other hand, does not include dispatching the integer and binary variables of the legacy devices as well as the optimal droop and modes of SIs and can therefore be formulated as an NLP problem, which requires solving (11) subject to (18).

$$\text{Stage-1:} \begin{cases} SIM_i \in [m_1 .... m_5], \quad \forall i \in \mathcal{N}_{pv} \\ SIS_i \in [V_i^L \dots V_i^H, \phi_i], \quad \forall i \in \mathcal{N}_{pv} \\ tp_i \in [-16, ..., +16], \quad \forall i \in \mathcal{N}_{tp} \\ Q_i^c = q_i^c\, tc_i, \quad \forall i \in \mathcal{N}_C \quad \text{where} \quad tc_i \in [0,1] \\ (1)-(10), (12)-(16) \end{cases} \tag{17}$$

$$\text{Stage-2:} \begin{cases} SIM_i = SIM_i^{opt} \quad \forall i \in \mathcal{N}_{pv} \\ SIS_i = [V_i^L \dots V_i^H, \phi_i]^{opt} \quad \forall i \in \mathcal{N}_{pv} \\ tp_i = tp_i^{opt} \quad \forall i \in \mathcal{N}_{tp} \\ Q_i^c = q_i^c\, tc_i^{opt} \quad \forall i \in \mathcal{N}_C \\ P_i^{min} \le P_i^G \le P_i^{pv}, \quad \forall i \in \mathcal{N}_{pv} \\ -Q_i^{pv} \le Q_i^G \le Q_i^{pv}, \quad \forall i \in \mathcal{N}_{pv} \\ (12)-(16) \end{cases} \tag{18}$$

where m is the SI modes, q_i^c reactive power rating of the capacitors, $\mathcal{N}_C$ is the set of nodes with CAPs, $\mathcal{N}_{tp}$ Set of branches with OLTC, SIS and SIS^{opt} are the set of SI setting and optimal setting, while SIM and SIM^{opt} set of SI modes and optimal modes.

IV. Coordination of Legacy Devices and SIs

This paper proposes a two-stage D-OPF for voltage optimization which uses five SI modes, namely: Volt/Watt, Volt/VAr P-priority, Volt/VAr Q-priority, CPF leading and CPF lagging in coordination with control of OLTCs and CAPs. The control variables of the first stage are the five modes of the SIs, the breakpoints of the SI droop based on the modes, the PF values (for SI CPF mode), the OLTC settings, and the CAPs status. The algorithm starts by solving a 1-hour resolution D-OPF using the defined first-stage control variables with the objective function defined as expressed in (11). The optimization results of the first-stage (SIM_i^{opt}, SIS_i^{opt}, tc_i^{opt} and tp_i^{opt}) are passed on to the second stage D-OPF. The second stage D-OPF is solved using the values of SIM_i^{opt}, SIS_i^{opt}, tc_i^{opt} and tp_i^{opt} with the active power and reactive power setpoint of SIs as the optimization control variables at a 1-minute resolution. Using the hourly optimal values for the first-stage D-OPF, the second stage is solved 60 times, after which the first-stage D-OPF is solved again for the next hour. The pseudo-code for the proposed D-OPF is presented in Algorithm 1.

Algorithm 1 Proposed D-OPF algorithm

procedure SOLVE FOR $SIM_i^{opt}, SIS_i^{opt}, tp_i^{opt}, tc_i^{opt}, Q_{i,t}^G, P_{i,t}^G \; \forall i \in \mathcal{N}_{pv}, \mathcal{N}_C, \mathcal{N}_{tp}$
  Begin time T=1
  Begin time t=1
  while $T \le 24$ **do** ▷ Solve 1-hr D-OPF
    Solve (11) s.t. (17) ▷ $SIM_{i,T}^{opt}, SIS_{i,T}^{opt}, tp_{i,T}^{opt}, tc_{i,T}^{opt}$
    while $t \le 60 \times t$ **do** ▷ Solve 1-min D-OPF
      Solve (11) s.t. (18) ▷ Solve Q_i^G,P_i^G
      if $t = T \times 60$ **then**
        T=T+1
        Execute step 4
      else
        t=t+1
        Execute step 6
      end if
    end while
  end while
end procedure

V. Simulation Results and Analysis

The IEEE 123-node, as shown in Fig. 3, is used to validate the effectiveness of the proposed algorithm. The feeder has a nominal voltage of 4.16 kV with four voltage regulators and four CAPs. The CAPs include one 600 kVAr three-phase

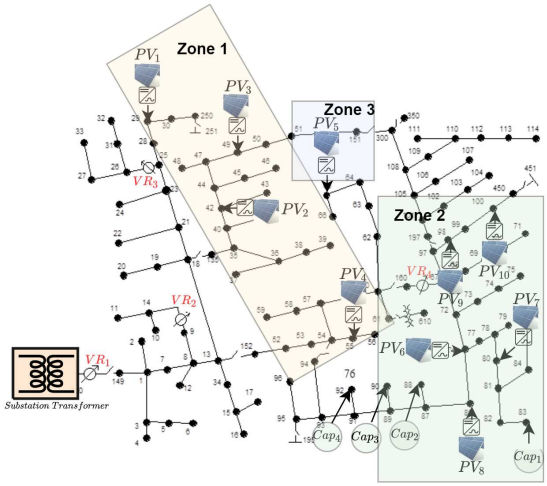

Fig. 3: IEEE 123 test node system with ten PVs integrated.

and three 50 kVAr single-phase. Ten units of PV systems rated 100 kW are integrated into the feeder. The PV's SIs were sized at 125% of the maximum DC capacity of the PVs. For the Volt/VAr (P-priority), the maximum $Q_i^G = \frac{\sqrt{1.25^2-1^2}}{1.25} = 0.6$ [12] while for the Volt/VAR (Q-priority), the maximum $Q_i^G \leq S_i^{SI}$ [13]. It is worthy of note that in the Volt/VAR (Q-priority) mode, the SI is allowed to curtail the active power as much as required by the setting $Q_i^G \leq S_i^{SI}$. Each SI is allowed to take five modes described earlier. An hourly sampled PV generation profile is used to dispatch the optimal VR, CAPs status, and SI modes and settings. In contrast, the 1-minute resolution PV generation profile is used for the dispatch of the SI's active and reactive power.

A. Optimal Tap Positions and CAPs Status

The optimal tap positions for VR_1, VR_2, VR_3, and VR_4 are as shown in Fig. 4.

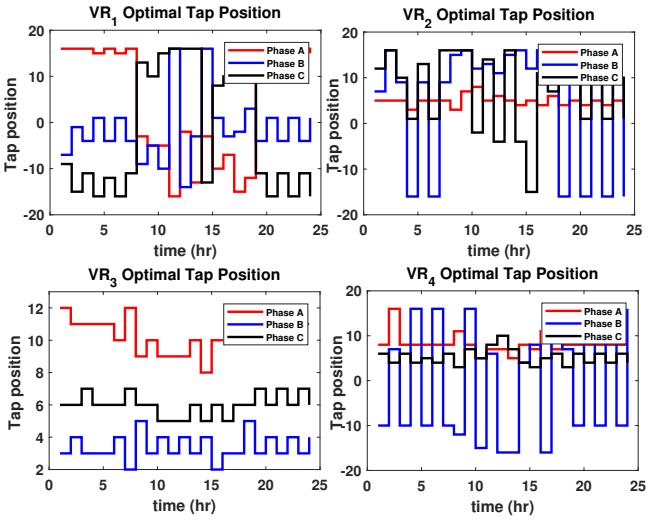

Fig. 4: Optimal tap positions for VR_1, VR_2, VR_3 and VR_4.

The summary of the tap changes for the four voltage regulators is tabulated in Table I. The total tap changes made by the four regulators during the 24hr period is 230. The total number of ON and OFF states of the four capacitor banks in the network during the 24hr period is as presented in Table II

TABLE I: OLTC/VR tap changes

	Ph A	Ph B	Ph C
VR_1	20	23	21
VR_2	19	23	21
VR_3	10	20	16
VR_4	12	22	23
Total	230		

TABLE II: Total number of CAPs ON/OFF status

$\sum_1^{24} tc_{i,T}^{opt}$	
ON	76
OFF	20

B. Optimal SI Modes and Settings

cThe optimal SI modes and settings for stage-one of D-OPF are as shown in Fig. 5. The modes and SI settings are plotted for the periods of PV power generation between 8 am to 4 pm. As seen in Fig. 5, the algorithm effectively selects the optimal modes of the SIs for each hour. All the possible SI modes (Volt/Watt, Volt/VAr (P-priority), Volt/VAr (Q-priority), CPF (leading and lagging)) considered during the optimization are used by the SIs for effective voltage regulation. During this period, the 10 SIs used CPF mode 38 times, VW mode 9 times, VV (P-priority) mode 13 times, and VV (Q-priority) 30 times.

C. Comparison with an Existing Method

In order to validate the effectiveness of the proposed D-OPF algorithms, a base-case scenario is set using the method proposed in [9, 14]. The authors in [9, 14] proposed some voltage sensitivity-based approaches to determine the SI modes based on their proximity to the feeder substation and the X/R ratio at the point of common coupling. Using their approach, the 10 PVs were categorized into three zones, as shown in Fig. 3. PV_1 to PV_4 in zone 1 is set at VV, PV_6 to PV_{10} in zone 2 is set at VW while PV_5 is set at CPF (with pf = 0.9 leading since the calculated pf is 0.7481). The droop settings of the VV and VW modes are selected without optimization but comply with IEEE 1547-2018. The voltage profile of all the PVs using the proposed D-OPFs and the base-case using the approach in [9, 14] is extracted. The variance of the phase voltages of each PV is computed and shown in Fig. 6. The variance values indicate the measure of the variability (dispersion) of each phase voltage of each PV system. As seen in fig. 6, the variability of the phase A voltage is less for 7 of the 10 PVs for D-OPF compared to that of the base-case. Also, for phases B and C, the variabilities of all the PVs using the proposed D-OPF are significantly less than that of the base-case. These results show the benefits of optimally selecting the modes and the droop settings of the SIs and properly coordinating them with the legacy devices for effective voltage control.

VI. Conclusion and Future Work

This paper presented a two time-scale distribution-grid optimal power flow (D-OPF) framework to optimally dispatch the mode (Volt/Watt, Volt/VAr P-priority, Volt/VAr Q-priority, constant power factor) and droop settings of smart inverters (SIs) as per the IEEE-1547. The first formulation allows the SI mode, SI settings, VR tap position, and capacitor bank status to be optimally determined on an hourly basis, while the optimal active and reactive power is dispatched on a 1-minute basis. The results show (in comparison with other SI modes and droop selection methods in literature)

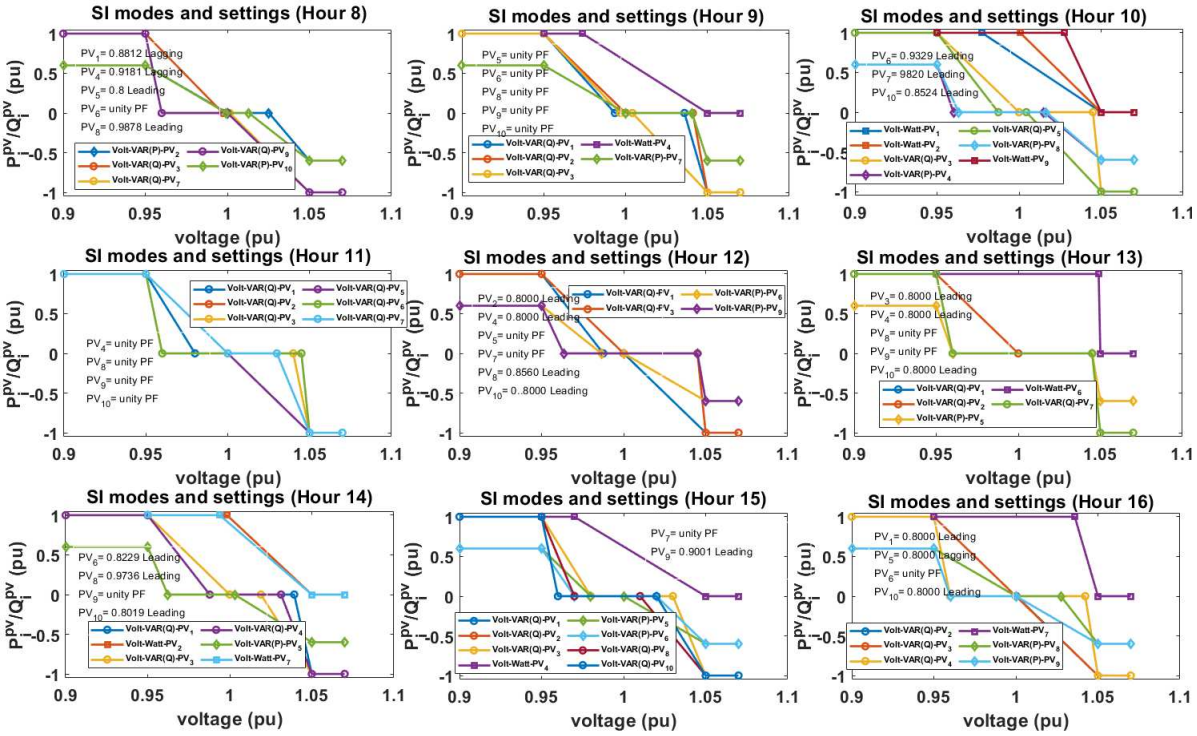

Fig. 5: Optimal SI modes and settings.

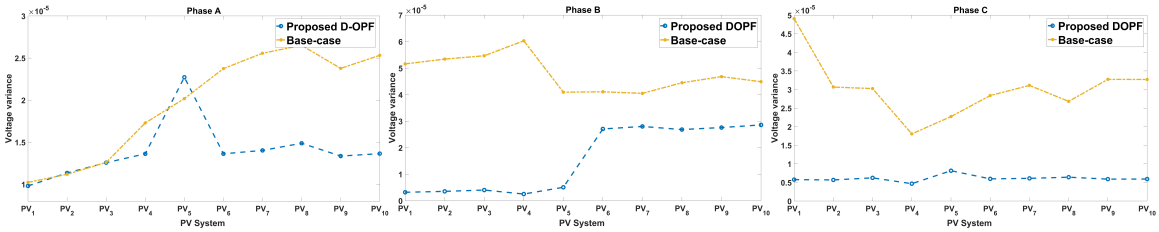

Fig. 6: Variance of the phase voltages of each PV.

the effectiveness and feasibility of proposed algorithms in optimally setting the droop and mode of SIs in coordination with legacy grid control devices for optimal voltage regulation. Since the proposed D-OPF formulation uses the non-linear grid model, the formulation may not be scalable for larger grid systems. As a future work, some linear approximations will be implemented on the proposed models in order to improve their scalability.

REFERENCES

[1] D. G. Photovoltaics and E. Storage, "IEEE standard for interconnection and interoperability of distributed energy resources with associated electric power systems interfaces," *IEEE Std*, pp. 1547–2018, 2018.

[2] Y. Long and D. S. Kirschen, "Bi-level volt/var optimization in distribution networks with smart PV inverters," *IEEE Transactions on Power Systems*, vol. 37, no. 5, pp. 3604–3613, 2022.

[3] F. U. Nazir, B. C. Pal, and R. A. Jabr, "Affinely adjustable robust volt/var control without centralized computations," *IEEE Transactions on Power Systems*, vol. 38, no. 1, pp. 656–667, 2023.

[4] A. Inaolaji, A. Savasci, and S. Paudyal, "Distribution grid optimal power flow in unbalanced multi-phase networks with volt-var and volt-watt droop settings of smart inverters," *IEEE Transactions on Industry Applications*, 2022.

[5] P. Lusis, L. L. Andrew, A. Liebman, and G. Tack, "Interaction Between Coordinated and Droop Control PV Inverters," in *Proc. Eleventh ACM International Conference on Future Energy Systems*, 2020, pp. 314–324.

[6] A. Savasci, A. Inaolaji, and S. Paudyal, "Two-stage volt-var optimization of distribution grids with smart inverters and legacy devices," *IEEE Transactions on Industry Applications*, vol. 58, no. 5, pp. 5711–5723, 2022.

[7] A. Inaolaji, A. Savasci, and S. Paudyal, "Optimal Droop Settings of Smart Inverters," in *Proc. IEEE 48th Photovoltaic Specialists Conference (PVSC)*. IEEE, 2021, pp. 2584–2589.

[8] I. Murzakhanov, S. Gupta, S. Chatzivasileiadis, and V. Kekatos, "Optimal design of volt/var control rules for inverter-interfaced distributed energy resources," *arXiv preprint arXiv:2210.12805*, 2022.

[9] M. Rylander, M. J. Reno, J. E. Quiroz, F. Ding, H. Li, R. J. Broderick, B. Mather, and J. Smith, "Methods to determine recommended feeder-wide advanced inverter settings for improving distribution system performance," in *Proc. IEEE 43rd Photovoltaic Specialists Conference (PVSC)*, 2016, pp. 1393–1398.

[10] J. Giraldez, M. Emmanuel, A. Hoke, and S. Suryanarayanan, "Impacts of voltage-based grid support functions on energy production of PV customers," in *Proc. 2019 IEEE Power Energy Society General Meeting (PESGM)*, 2019, pp. 1–5.

[11] Z. Yang, H. Zhong, A. Bose, Q. Xia, and C. Kang, "Optimal power flow in ac–dc grids with discrete control devices," *IEEE Transactions on Power Systems*, vol. 33, no. 2, pp. 1461–1472, 2018.

[12] R. A. Jabr, "Robust volt/var control with photovoltaics," *IEEE Transactions on Power Systems*, vol. 34, no. 3, pp. 2401–2408, 2019.

[13] J. Seuss, M. J. Reno, R. J. Broderick, and S. Grijalva, "Analysis of PV advanced inverter functions and setpoints under time series simulation," *Sandia National Laboratories SAND2016-4856*, 2016.

[14] J. Smith, M. Rylander, J. Boemer, R. J. Broderick, M. J. Reno, and B. Mather, "Analysis to inform ca grid integration rules for PV: Final report on inverter settings for transmission and distribution system performance," 9 2016. [Online]. Available: https://www.osti.gov/biblio/1431468